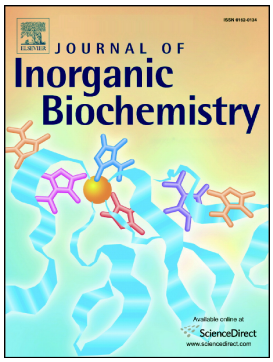

Tris-heteroleptic ruthenium(II) polypyridyl complexes: Synthesis, structural characterization, photophysical, electrochemistry and biological properties

Satish S. Bhat, Avinash S. Kumbhar, Neeraja Purandare, Ayesha Khan, Günter Grampp, Peter Lönnecke, Evamarie Hey-Hawkins, Ruchi Dixit, Kumar Vanka

PII: S0162-0134(19)30366-6

DOI: https://doi.org/10.1016/j.jinorgbio.2019.110903

Reference: JIB 110903

To appear in: *Journal of Inorganic Biochemistry*

Received date: 4 June 2019

Revised date: 14 October 2019

Accepted date: 18 October 2019

Please cite this article as: S.S. Bhat, A.S. Kumbhar, N. Purandare, et al., Tris-heteroleptic ruthenium(II) polypyridyl complexes: Synthesis, structural characterization, photophysical, electrochemistry and biological properties, *Journal of Inorganic Biochemistry* (2019), https://doi.org/10.1016/j.jinorgbio.2019.110903

Tris-Heteroleptic Ruthenium(II) Polypyridyl Complexes: Synthesis, Structural Characterization, Photophysical, Electrochemistry and Biological Properties

Satish S. Bhat,[a] Avinash S. Kumbhar,*[a] Neeraja Purandare,[b] Ayesha Khan,[b] Günter Grampp,[c] Peter Lönnecke,[d] Evamarie Hey-Hawkins[d] Ruchi Dixit[e] and Kumar Vanka[e]

[a] Department of Chemistry, Savitribai Phule University of Pune, Pune-411007, India

[b] Institute of Bioinformatics and Biotechnology, Savitribai Phule Pune University of Pune, Pune- 411007, India.

[C] Institute of Physical and Theoretical Chemistry, Technical University Graz, A-8010, Austria.

[d] Faculty of Chemistry and Mineralogy, Institute of Inorganic Chemistry, Johannisallee-29, Universität Leipzig, 04103 Leipzig, Germany.

[e] Physical and Materials Chemistry division, CSIR - National Chemical Laboratory, pune, 411008, India.

* Corresponding authors

E-mail: askum@chem.unipune.ac.in

Abstract

Three water-soluble tris-heteroleptic ruthenium(II) polypyridyl complexes $[Ru(bpy)(phen)(bpg)]^{2+}$ (**1**), $[Ru(bpy)(dppz)(bpg)]^{2+}$ (**2**), and $[Ru(phen)(dppz)(bpg)]^{2+}$ (**3**) (where bpy = 2,2′-bipyridine, phen = 1,10-phenanthroline, dppz = dipyrido[3,2-a:2',3'-c] phenazine, bpg = 4*b*,5,7,7*a*-tetrahydro-4*b*,7*a*-epiminomethanoimino-*6H*-imidazo[4,5-*f*] [1,10] phenanthroline-6,13-dione) have been synthesized and characterized. Molecular structures of complexes **1** and **3** are confirmed by single crystal X-ray structure determination. Interaction of complexes **1**-**3** with DNA is explored by various spectroscopic techniques. The complexes 1-3 show solvent dependent photophysical properties. Complexes **2** and **3** show extensive "molecular light switch" effect for DNA. The complexes **1**-**3** are low toxic towards HeLa (human cervical cancer) and HL-60 (human promyelocytic leukaemia) cell lines. Further, the cellular uptake of complexes **2** and **3** by cells shows that complexes mainly localised on the nucleus of the cells.

Keywords: ruthenium• polypyridyl• fluorescence• circular dichroism • cytotoxicity

1. Introduction

Luminescent molecules having low toxicity and ability to undergo cellular uptake are of great importance as molecular probes for cellular imaging, across cell biology, molecular biology, and flow cytometry applications[1-3]. The understanding of DNA structure and organization within the cell is of great importance as DNA is a carrier of genetic material[3]. For this purpose, biologists are using organic dyes which have major disadvantages such as low water solubility, high toxicity, photo bleaching effect, small Stokes shift and require UV light irradiation leading to cleavage of DNA[4-6]. Another main task in cellular imaging is to differentiate the endogenous fluorescence of biological species (auto-fluorescence) from that of the organic dyes which are applied. If the fluorophore dye has the large stoke shift then the auto-fluorescence can be eliminated from the required signal because the typical Stokes shifts for species involved in auto-fluorescence is small[4-6]. Additionally, the auto-fluorescence can be eliminated if the emission lifetime of the fluorophore is much longer than the short-lived auto-fluorescence by using time-resolved microscopy. However, it is still difficult to differentiate the area occupied by the fluorophore autofluorescence[6-8].

In this context, the exceptional photophysical properties such as intense polarized luminescence, large Stokes shift, high water solubility, red emission wavelength, and good photostability of ruthenium(II) polypyridyl complexes make them potentially valuable probes for cellular imaging and probe for DNA structure determination [3, 9-22]. The Ruthenium(II) dipyridophenazine complexes {$[Ru(NN)_2(dppz)]^{2+}$, NN = 2,2′-bipyridine (bpy), 1,10-phenanthroline (phen), dipyrido[3,2-a:2′,3′-c]phenazine (dppz) has low background emission and long emission life time, when bound to DNA, make them attractive candidates as molecular probes for cellular imaging using fluorescence microscopy[10, 23]. J. A. Thomas et.al. have reported the dinuclear ruthenium(II) polypyridyl complex as an *in cellulo* nuclear stain for eukaryotic and prokaryotic cells[3, 24]. Research on ruthenium polypyridyl complexes has mainly focused on the design of *in vitro* probes, but the use of these complexes in cellular imaging of nucleic acids in cells is limited due to poor cell membrane permeability and structure-specific binding[3, 10, 12, 21, 25-29]. Recently Liang-Nian Ji and coworker have reported the effect of modification of ancillary ligand on DNA binding modes and cytotoxicity of ruthenium complexes[13, 14, 30].

As a part of our project aimed to investigate the effect of modification of ancillary ligands of ruthenium complexes on DNA interaction properties, we previously demonstrated the DNA binding and DNA condensation properties of the complexes[24, 31-36]. Herein, we report on structural, photophysical, electrochemical, DNA binding and cellular imaging properties of three new tris-heteroleptic ruthenium(II) polypyridyl systems (Scheme 1).

2.0 Results and Discussion

2.1 Synthesis and Characterization

Tris-heteroleptic ruthenium(II) polypyridyl complexes were synthesized as shown in Scheme 1 by reacting appropriate ligands followed by chromatographic purification using neutral alumina column and obtained as racemic mixtures. The compounds were characterized by NMR, IR, elemental analysis, UV–Visible spectroscopy and electrospray mass spectrometry (see experimental section). In ESI-MS (Electrospray Ionization Mass Spectrum) spectra peaks due to $[M - Cl]^+$ and $[M - 2Cl]^{2+}$ were observed. Complexes **1** and **3** were characterized by single-crystal X-ray structure analysis. Further physicochemical and biological studies were carried out using the racemic mixtures.

2.2 Single Crystal Structures

Single crystals of complexes **1** and **3** suitable for single-crystal X-ray data collection were grown by slow evaporation of complexes dissolved in dimethylsulfoxide/water and methanol/water, respectively. Relevant crystallographic information for complexes **1** and **3** is given in Table S1 (Supporting Information), and a list of selected bond lengths and angles can be found in Tables 1 and 2. ORTEP (Oak Ridge Thermal Ellipsoisal Plot) representations of ruthenium complexes **1** and **3** are shown in Figure 1. Both complexes crystallize in the monoclinic space group $P2_1/c$. The ruthenium(II) cation is chelated by three different polypyridyl ligands namely bpy, phen and bpg for complex **1**, and phen, dppz and bpg in case of complex **3**. The N-Ru-N "bite" angles for the bidentate ligands are 83.00(3), 75.80(3), 79.1(1)° for complex **1**, and 80.0(2), 79.5(2), 79.2(2)° for complex **3**, which are typical of 5-membered chelate rings formed by such diimine ligands[11, 22, 37-40]. The mean Ru-N (phen) bond length is 2.063 Å, the Ru-N (bpy) bond length of 2.074 Å and the Ru-N (bpg) (bpg= bpg = 4*b*,5,7,7*a*-tetrahydro-4*b*,7*a*-epiminomethanoimino-*6H*-imidazo[4,5-*f*] [1,10] phenanthroline-6,13-dione) bond length of 2.058 Å for complex **1** and is similar to that found in other analogous mixed ligand polypyridyl ruthenium(II) complexes[11, 22, 39, 40] including tris-heteroleptic ruthenium(II)-diimine complexes[37, 38]. The molecular structure of **3** shows "dimers" formed by intermolecular hydrogen donor and acceptor bonds between bpg ligands (Figure S4, Supporting Information).

2.3 Photo-physical Studies

The UV/Visible and emission data of complexes **1-3** in different solvents are summarized in Table 3 and the absorption and luminescence spectra of the complexes **1-3** are shown in Figure S5 and Figure S6 (Supporting Information). The low energy broad band around 450 nm for the complexes **1-3** is assigned to the MLCT (Metal to Ligand Charge Transfer) Ru ($d\pi$) $\rightarrow$ ligand (π^*) transitions[13, 32, 41] typical of polypyridyl ruthenium(II) complexes. The intense bands between 240 to 300 nm corresponding to $\pi \rightarrow \pi^*$ transitions of the aromatic polypyridyl ligands. In case of complexes **2** and **3** a band around 360 nm corresponds to the characteristic of a $\pi \rightarrow \pi^*$ (dppz) transition[32, 33, 35, 42].

Complexes **1-3** show strong luminescence in organic solvents with an emission peak centered between 600 and 750 nm but these complexes have weak emission in aqueous solutions. The emission maxima and quantum yield with respect to $[Ru(bpy)_3]^{2+}$ as standard are compiled in Table 3.

2.4 Electrochemistry

The oxidation and reduction potentials of the complexes in acetonitrile are compiled in Table 4. Complexes **1**-**3** exhibit one oxidation and three reduction waves in the sweep range from -2.0 to +2.0 V (Figure 2) and display ruthenium(II/III)-based half-wave oxidation potential at 0.96, 0.99, 0.99 versus $Fc^{0/+}$, respectively. The anodic shift relative to $[Ru(bpy)_3]^{2+}$ (0.88 V) is attributed to the more electronegative character or stronger π-accepting feature of the ligands that stabilize the ruthenium-based HOMO (Highest Occupied Molecular Orbital), rendering the oxidation of the metal more difficult, similar to other ruthenium(II) mixed polypyridyl complexes[13, 43-45]. All complexes exhibit three reversible or quasi-reversible redox couples. The ruthenium(II/III)-based half-wave oxidation potential of complex 2 and 3 are almost same due to the almost same HOMO to LUMO (Lowest Occupied Molecular Orbital) gap in both the complexes, which is evidenced by density functional theoretical calculation (discussed in electronic structure calculation section). Due to the similarity between the ligands used here, our data do not allow the order in which the ligands are reduced for either complex to be determined.

2.5 Spectroelectrochemistry

The bulk electrolysis experiments were conducted to further probe the metal-based (Ru^{II}/Ru^{III}) redox process. For each experiment, the oxidation of Ru^{II} to Ru^{III} *in situ* was followed by absorption spectroscopy by applying a constant potential of 200 mV higher than that of the oxidation potential (vs Fc/Fc^{+}) of the complex at a platinum gauze electrode to a 30 μM complex solution in acetonitrile. For complex **1**, a potential of 1120 mV (vs Fc/Fc^{+}) was applied to a platinum gauze electrode, and the oxidation of Ru^{II} to Ru^{III} *in situ* was monitored (Figure 3). In the absorption spectrum, the bands at 262 and 286 nm decreased in intensity accompanied by the growth of a band at 325 nm. In the visible region, the MLCT band at 454 nm decreased in intensity and the oxidized species display a weak band at 430 nm. Isosbestic points were observed at 356, 296, 269 and 256 nm indicating a clean oxidation reaction. After the potential was removed reconversion to $[Ru^{II}(bpy)(phen)(bpg)]^{2+}$ was not observed, even though low concentration of the complex was used. However, by changing the applied potential to 800 mV (vs Fc/Fc^{+}) almost complete reversion to $[Ru^{II}(bpy)(phen)(bpg)]^{2+}$ was achieved[37, 46]. The three bands observed in the high energy region for the electrogenerated Ru^{III} complex at 262 nm and 325 nm have been assigned to intra-ligand ($\pi \rightarrow \pi^*$) transitions of the diimine ligands[47, 48]. The weak band observed in

the visible region at 430 nm is attributed to an LMCT transition ($\pi \rightarrow t_2$) characteristic of Ru^{III}[36].

2.6 Electronic structure calculations

To probe the excitation in complexes **1**-**3** in comparison with reported $[Ru(bpy)_3]^{2+}$, $[Ru(bpy)_2(dppz)]^{2+}$ complexes a series of TD-DFT (Time Dependent Density Functional Theory) computations were carried out. The HOMO-LUMO energy level diagram is given in Figure 4. The UV-Vis absorption originates from HOMO to LUMO electronic transition, where HOMO is located on the metal center which has a significant amount of dz^2 character and LUMO is delocalized over the carbon ring with significant π- character. From the theoretically calculated first excitation energy (S0→S1) it has been found that the excitations occur almost at the same wavelength.

2.7 DNA BINDING STUDIES

2.7.1 Steady-state Emission Studies

The investigation of the interaction of the molecules with the DNA by monitoring the changes in the luminescence spectra are diagnostic means to determine the DNA binding[32, 36, 49]. In the aqueous buffer solution complexes, **1**-**3** show an increase in luminescence intensity with the successive addition of CT-DNA (Calf Thymus-DNA) (Figure 5). Complexes **2** and **3** shows negligible luminescence in aqueous solution, but in the presence of DNA are strongly luminescent displaying a "molecular light switch effect" (Figure 5) with luminescence enhancement of around 95-fold, indicating strong binding of these complexes with CT-DNA. However, complex **1** shows only a small increase in emission intensity around 1.2 times upon addition of DNA indicating weak binding. This implies that complexes **2** and **3** interact strongly with DNA by intercalation[23]. The dipyridophenazine (dppz) containing complexes **2** and **3** acts as "molecular light switch" for DNA due to intercalation of dppz ligand between the base pairs of CT-DNA this behaviour is similar to that observed for the complex {$[Ru(NN)_2(dppz)]^{2+}$, NN = 2,2′-bipyridine (bpy), 1,10-phenanthroline (phen), dipyrido[3,2-a:2′,3′-c]phenazine (dppz) in the presence of DNA[23]. The molecular light switch behavior of complexes **2** and **3** for DNA may be mainly due to two reasons: first, these complexes have dppz ligand with stack between base-pairs of DNA by intercalation mode of binding and the hydrophobic environment inside the DNA helix

reduces the accessibility of water molecules with the N-atom of the phenazine moieties of the complex, interaction of water molecules quenches the emission and second, the complex mobility is restricted at the binding intercalation binding site and so the vibrational mode of relaxation decreases[15-18].

DNA binding of these complexes with DNA was further confirmed by time-correlated single-photon counting luminescence measurements. For complex **1** no increase in lifetime was observed at [CT-DNA]: [Ru] = 20; complexes **2** and **3** do not have any fluorescence but in the presence of CT-DNA showed strong luminescence with emission lifetime of 1056 ns and 1078 ns, respectively, at [CT-DNA]: [Ru] = 20 confirming the strong binding of these complexes. A similar effect was found in other ruthenium polypyridyl complexes which exhibit a molecular light switch effect[23, 36].

2.7.2 Absorption Spectroscopy Studies

The interaction of molecules with DNA can be followed by absorption spectroscopy, which is one of the wide techniques to understand the mode of interaction of molecules with DNA.[32, 50] The interaction of molecules with the DNA through intercalation results in hypochromism and a redshift, due to the interaction of the complex and between the base pairs of the DNA[19, 32, 34, 35, 50-55]. The electronic spectra of complexes **2** and **3** in the presence and absence of DNA are shown in Figure S7 (supporting information), a redshift of the MLCT band by 10 nm and 6 nm, respectively, was observed for complexes **2** and **3** in the presence of DNA. The percentage of hypochromicity for the MLCT band of complex **2** (450 nm) and **3** (438 nm) upon binding to DNA was observed to be 15% and 12%, respectively (Table 5). The intrinsic binding constants of complexes **2** and **3** with CT-DNA were estimated from equation 2 (Supporting Information). The CT-DNA binding constants for thecomplexes **2** and **3** Figure S7 (supporting information) were found to be 2.3×10^4 and 6.8×10^4 M^{-1}respectively. These values are comparable to that of some known DNA intercalators such as 1.2×10^5 M^{-1} for $[Ru(NH_3)_4(dppz)]^{2+}$,[56] 3.9×10^5 M^{-1} for $[Ru(bpy)_2(dcdpq)]^{2+}$ (dcdpq = dicyano-dipyrido[3,2-*d*:2′,3′-*f*]quinoxaline),[57] 4.7×10^4 M^{-1} for $[Ru(bpy)_2(dpq)]^{2+}$,[55] 6.3×10^4 M^{-1} for $[Ru(bpy)_2(dpt)]^{2+}$ (dpt = 3-(pyrasinyl)- *as*-triazino[5,6-*f*]phenanthrene),[58] 4.9×10^4 M^{-1} for $[Ru(bpy)_2(aip)]^{2+}$ (aip = 2-(9-anthryl)-*1H*-imidazo[4,5-*f*][1,10] phenanthroline),[20] but smaller than that of the parent complex $[Ru(bpy)_2(dppz)]^{2+}$ ($K_b = 5.0\times10^6$ M^{-1})[13] probably due to hindrance caused by the non-planar bpg ancillary ligand for intercalative binding. The spectral characteristic of

hypochromism and redshifts, as well as large Kb values, suggest that the two complexes bind to DNA by partial intercalation mode. The complex **2** and **3** have higher DNA binding constants due to the presence of planar dppz ligand which intercalates between the base-pairs of DNA, but complex **1** planarity of the ligands bpy, bpg, and phen ligands is much less compared to dppz so this complex weakly interacts with DNA.

2.7.3 DNA Melting Experiments

The DNA helix melting temperature increases with the intercalation of small molecules into the double helix[32, 59-62]. The DNA melting temperature is the point where the double helix denatures into single-stranded DNA[32]. The double-stranded DNA has very small extinction coefficient at 260nm compared to the single-stranded form of DNA. Therefore, the melting of the helix leads to an increase in the absorption at this wavelength. In the absence of complex, CT-DNA melts at 65±1 °C (phosphate buffer). A large increase in melting temperature, 6 °C for **2** and 7 °C for **3**, was observed and is comparable to that observed for classical intercalators[59-62]. These results are consistent with the other spectroscopic studies indicating the intercalation of complexes **2** and **3** into the DNA helix.

2.7.4 Viscosity Studies

Intercalation of molecules with DNA is known to cause a substantial increase in viscosity of a DNA solution due to an increase in separation of base pairs at the intercalation site, and hence, an increase in overall DNA molecular length[32, 63, 64]. In contrast, a complex that binds to the DNA grooves causes less-pronounced changes or no change in viscosity of a DNA solution[63, 64]. Typical data of such experiments on complexes **1**-**3** in comparison with DNA intercalator ethidium bromide (EtBr) is shown in Figure 6. The complexes **1**, **2** and **3** induces viscosity changes that are indicative of stronger DNA binding and are similar to that of previously reported complexes[32, 64]. The viscosity changes for complex **2** and **3** are similar to that of well-known DNA intercalator ethidium bromide suggesting intercalation mode of DNA binding by complexes **2** and **3**. These results are inconsistent with absorption and emission titration, and thermal melting experiments showing stronger binding of complexes **2** and **3** to the DNA by intercalation.

2.7.5 Circular Dichroism (CD) Spectral Analysis

The conformational changes in the DNA by the interaction of molecules with the DNA can be investigated by CD spectral analysis[65-67]. To confirm the interaction of complexes **1-3** with DNA, CD spectra of DNA were recorded in the presence and absence of complexes **1**-**3**. A very small change in the CD spectrum of DNA was observed when complex **1** was added to DNA due to an electrostatic mode of interaction (Figure 7). Addition of complexes **2** or **3** to DNA increased the intensity of the positive band which may be due to strong interactions (Figure 7). These results show that complexes **2** and **3** interact with DNA and change their conformation.

2.7.6 Cytotoxicity Studies

Low toxicity is a prerequisite for cellular imaging probes for long-term monitoring. Hence toxicity profiles for complexes 1-**3** were evaluated by MTT {3-(4,5-dimethylthiazol-2-yl)-2,5-diphenyl tetrazolium bromide} assay against HeLa (human cervical cancer) and HL-60 (human promyelocytic leukemia) cell lines (Figure 8 and Figure 9). Complexes **1-3** did not display noticeable cytotoxicity towards both cell lines; cell viability is more than 80 % even after 72 h incubation of cells with complexes **1-3**, and after 24 h of incubation rapid growth of cells is observed, hence there is an increase in cell viability. The low toxicity of the complexes may be due to the electrostatic binding by complex **1** and low order of DNA binding constant of the complexes of the order 10^4 for complexes **2** and **3**.

2.7.7 Cellular Imaging Studies

The cellular uptake and localization properties of complexes **1**-**3** were evaluated using fluorescence microscopy. For fluorescence microscopy experiments the cells were treated with complexes **2** and **3** and co-stained with DAPI (DAPI = 4′,6-diamidino-2-phenylindole) for 24 and 72 h. Both complexes undergo rapid cellular internalization and clearly visible within the cell after 24 h incubation (Figure 10 and 11). To a co-staining experiment with the DNA-specific dye DAPI was performed and strong co-localization of complex signal with that of DAPI was observed (Figure 10 and 11, overlay image, and Figure S8 and S9, Supporting Information). From these studies, it is proposed that complexes **2** and **3** can be used as potential DNA-staining probes.

3.0 Conclusions

In summary, three novel non-toxic water-soluble tris-heteroleptic ruthenium(II) polypyridyl complexes **1**-**3** have been designed, and the photophysical and electrochemical properties have been investigated. Electrochemical studies of **1**-**3** showed a reversible Ru^{II}/Ru^{III} oxidation process at 0.96, 0.99, 0.99 V (vs Fc/Fc^{+}), respectively. The complexes **2** and **3** show an extensive "molecular light switch effect" for DNA. The DNA binding significantly stronger for the complexes **2** and **3** than the complex **1**. The complexes **1**-**3** are low toxic towards HeLa and HL-60 cell lines. Further, the complexes **2** and **3** specifically stains the nucleus of the cells.

4.0 Experimental Section

4.1 Chemicals

All chemicals and solvents were purchased commercially and were used as received. $RuCl_3 \cdot 3H_2O$ was purchased from S. D. Fine Chemicals, Mumbai and calf thymus DNA was purchased from SRL, Kolkata and used as received.

4.2 Synthesis

The ligands 1,10-phenanthroline-5,6–dione (phendione),[68] and dipyrido[3,2-*a*:2′,3′-*c*] phenazine (dppz),[69, 70] 4*b*,5,7,7*a*-tetrahydro-4*b*,7*a*-epiminomethanoimino-6*H*-imidazo[4,5-*f*][1,10]phenanthroline-6,13-dione (bpg),[71, 72] $[RuCl_2(dmso)_4]$[73] and $[Ru(NN)(NN)'Cl_2)]$ (where, NN, NN′ are different polypyridine ligands) were synthesized according to the literature[74].

4.2.1 $[Ru(bpy)(phen)(bpg)]Cl_2$ (1)

The precursor complex *cis*-$[Ru(bpy)(phen)Cl_2] \cdot 2H_2O$ (100 mg, 0.196 mmol) and bpg (57 mg, 0.196 mmol) were dissolved in methanol-water (1:1, 50 mL) and the mixture was heated to reflux for 8 h, whereupon the color of the solution changed from dark purple to red. The red solution was filtered hot and was cooled to room temperature. The solvent was removed under vacuum to obtain a red solid. The product was purified by column chromatography on neutral alumina using acetone and methanol as solvents. The orange-red fraction was collected and concentrated under vacuum to get the orange-red pure product. Yield: 130 mg (82.3%). Crystals were grown by slow evaporation of a solution of the perchlorate salt of the complex which was prepared by adding aqueous sodium perchlorate

solution to the purified product in water. The bright red precipitate formed was collected by filtration and washed with diethyl ether. ^{1}H NMR (DMSO-d_6, 300 MHz, 25 °C); δ = 8.84 (m, 5H), 8.72 (t, 2H), 8.46 (t, 2H), 8.38 (s, 2H), 8.22 (m, 3H), 8.11 (m, 2H), 7.89 (m, 2H), 7.79 (d, 1H), 7.69-7.43 (m, 6H), 7.35 (t, 1H); IR (KBr pellet, cm^{-1}) $\tilde{\nu}$ = 3448 (H_2O), 3176 (NH), 3101, 3084 (ArH), 1707 (C=O), 1635, 1608, 1454, 1423 (C=C, C=N); ESI-MS (m/z, positive mode) : ([M–2Cl]$^{2+}$) 366 (~100), ([M–2Cl–H]$^+$) 731 (~5%); Anal. Calcd. for $C_{36}H_{26}N_{10}O_2Cl_2Ru\cdot 4H_2O$: C, 49.41; H, 3.92; N, 16.02; found: C, 49.19 ; H, 4.01; N, 16.23.

Caution!! Perchlorate salts of metal complexes with organic ligands are potentially explosive, and only small amounts of material should be prepared and these should be handled with great care.

4.2.2 [Ru(bpy)(dppz)(bpg)]Cl_2 (2)

The synthesis and purification of compound **2** was similar to that of **1** using *cis*-[Ru(bpy)(dppz)Cl_2]·2H_2O (100 mg, 0.164 mmol) and bpg (48 mg, 0.164 mmol). Yield: 95 mg (64.2%). ^{1}H NMR (DMSO-d_6, 300 MHz, 25 °C); δ = 9.64 (dd, 2H), 8.86 (t, 2H), 8.74 (d, 2H), 8.52 (m, 4H), 8.34 (m, 2H), 8.25-8.12 (m, 6H), 8.08 - 8.01 (m, 2H), 7.89 (d, 2H), 7.78 - 7.62 (m, 4H), 7.51 (m, 1H), 7.39 (t, 1H); IR (KBr pellet, cm^{-1}); $\tilde{\nu}$ = 3416 (H_2O), 3217 (NH), 3090, 2924 (ArH), 1703 (C=O), 1649, 1456, 1384 (C=C, C=N).; ESI-MS: (m/z, (% positive mode): ([M–2Cl–H]$^+$) 833 (~7%), ([M–2Cl]$^{2+}$) 417 (~100%); Anal. Calcd. for $C_{42}H_{28}N_{12}O_2Cl_2Ru\cdot 2.5H_2O$; C, 53.12; H, 3.54; N, 17.69; found: C, 53.27; H, 3.49; N, 17.41.

4.2.3 [Ru(phen)(dppz)(bpg)]Cl_2 (3)

The synthesis and purification of compound **3** was similar to that of **1** using *cis*-[Ru(phen)(dppz)Cl_2]·2H_2O (100 mg, 0.157 mmol) and bpg (46 mg, 0.157 mmol). Yield: 88 mg (60.2%). Crystals were grown by slow evaporation of solution of complex in water:methanol mixture. ^{1}H NMR (DMSO-d_6, 300 MHz, 25 °C) δ = 9.68 (d, 1H), 9.57 (d, 1H), 8.86 (d, 1H), 8.74 (m, 3H), 8.52 (m, 3H), 8.44 (d, 2H), 8.40 (d, 2H), 8.29 (d, 2H), 8.19-8.07 (m, 5H), 8.05-7.97 (m, 2H), 7.85 (m, 2H), 7.76 (m, 1H), 7.64-7.50 (m, 3H); IR (KBr pellet, cm^{-1}); $\tilde{\nu}$ = 3456 (H_2O), 3209 (NH), 3091 2924 (ArH), 1701 (C=O), 1651, 1433, 1373 (C=C, C=N).; ESI-MS: (m/z, (%) positive mode): ([M–Cl]$^+$) 894 (~7%), ([M–2Cl]$^{2+}$) 429 (~100%); Anal. Calcd. for $C_{44}H_{28}N_{12}O_2Cl_2Ru\cdot 3H_2O$: C, 53.77; H, 3.49; N, 17.11; found: C, 53.62; H, 3.61; N, 16.93.

4.3 Methods and Instrumentation

Details of instruments used and the methods/bioassays are given in supplementary material.

4.4 Supporting Information. Relevant crystallographic information for complexes **1** and **3** is given in Table S1. ESI-MS spectra of complexes **1-3** (Figures S1-S3), Packing diagram of **3** (Figure S4), absorption spectra of complexes **1-3** (Figure S5), emission spectra of complexes **1-3** (Figure S6), Absorption titration with DNA (Figure S7), fluorescence microscopy images after 72 h incubation (Figures S8 and S9).

5.0 Table of Abbreviations:

bpy = 2,2′-bipyridine
phen = 1,10-phenanthroline
dppz = dipyrido[3,2-a:2',3'-c] phenazine
bpg = 4*b*,5,7,7*a*-tetrahydro-4*b*,7*a*-epiminomethanoimino-*6H*-imidazo[4,5-*f*] [1,10] phenanthroline-6,13-dione
ESI-MS = Electrospray Ionization Mass Spectrum
CT-DNA = Calf Thymus – DNA
ORTEP = Oak Ridge Thermal Ellipsoisal Plot
MLCT =Metal to Ligand Charge Transfer
HOMO = Highest Occupied Molecular Orbital
LUMO = Lowest Occupied Molecular Orbital
TD-DFT = Time Dependant Density Functional Theory
MTT ={3-(4,5-dimethylthiazol-2-yl)-2,5-diphenyl tetrazolium bromide}
EtBr = ethidium bromide
CD = Circular Dichroism
HeLa = human cervical cancer
HL-60 = human promyelocytic leukemia
DAPI = 4′,6-diamidino-2-phenylindole

6.0 Acknowledgements

SSB acknowledges the Department of Science and Technology (DST), New Delhi, India, for providing a fellowship under the scheme SR/S5/BC-25/2006. ASK acknowledges the Department of Science and Technology (DST), New Delhi, India, for financial support under

"New Initiatives in Bioinorganic Chemistry" (SR/S5/BC-25/2006). A.S.K. and E. H-H. acknowledges financial support from the Indo-German (DST-DAAD) joint Research Project (INT/FRG/DAAD/P-225/2013). SSB acknowledges the OEAD fellowship for short term research visit to the Graz University of Technology. We thank SAIF, CDRI-Lucknow, India for providing ESI-MS data.

7.0 References

[1] E. Baggaley, M.R. Gill, N.H. Green, D. Turton, I.V. Sazanovich, S.W. Botchway, C. Smythe, J.W. Haycock, J.A. Weinstein, J.A. Thomas, Angewandte Chemie International Edition, 53 (2014) 3367-3371.

[2] Q. Zhao, C. Huang, F. Li, Chemical Society Reviews, 40 (2011) 2508-2524.

[3] M.R. Gill, J. Garcia-Lara, S.J. Foster, C. Smythe, G. Battaglia, J.A. Thomas, Nature Chemistry, 1 (2009) 662.

[4] R.M. Martin, H. Leonhardt, M.C. Cardoso, Cytometry Part A, 67A (2005) 45-52.

[5] U. Neugebauer, Y. Pellegrin, M. Devocelle, R.J. Forster, W. Signac, N. Moran, T.E. Keyes, Chemical Communications, (2008) 5307-5309.

[6] A.J. Amoroso, M.P. Coogan, J.E. Dunne, V. Fernandez-Moreira, J.B. Hess, A.J. Hayes, D. Lloyd, C. Millet, S.J.A. Pope, C. Williams, Chemical Communications, (2007) 3066-3068.

[7] M. Neumann, D. Gabel, Journal of Histochemistry & Cytochemistry, 50 (2002) 437-439.

[8] Principles of Fluorescence Spectroscopy, Third ed., Springer US, New York, US, 2006.

[9] M.R. Gill, J.A. Thomas, Chemical Society Reviews, 41 (2012) 3179-3192.

[10] C.A. Puckett, J.K. Barton, Journal of the American Chemical Society, 129 (2007) 46-47.

[11] A. Ghosh, A. Mandoli, D.K. Kumar, N.S. Yadav, T. Ghosh, B. Jha, J.A. Thomas, A. Das, Dalton Transactions, (2009) 9312-9321.

[12] M.R. Gill, D. Cecchin, M.G. Walker, R.S. Mulla, G. Battaglia, C. Smythe, J.A. Thomas, Chemical Science, 4 (2013) 4512-4519.

[13] J.-G. Liu, Q.-L. Zhang, X.-F. Shi, L.-N. Ji, Inorganic Chemistry, 40 (2001) 5045-5050.

[14] H. Xu, K.-C. Zheng, H. Deng, L.-J. Lin, Q.-L. Zhang, L.-N. Ji, New Journal of Chemistry, 27 (2003) 1255-1263.

[15] E.J.C. Olson, D. Hu, A. Hörmann, A.M. Jonkman, M.R. Arkin, E.D.A. Stemp, J.K. Barton, P.F. Barbara, Journal of the American Chemical Society, 119 (1997) 11458-11467.

[16] M.K. Brennaman, J.H. Alstrum-Acevedo, C.N. Fleming, P. Jang, T.J. Meyer, J.M. Papanikolas, Journal of the American Chemical Society, 124 (2002) 15094-15098.

[17] J. Olofsson, B. Önfelt, P. Lincoln, The Journal of Physical Chemistry A, 108 (2004) 4391-4398.

[18] C. Qian, J. Wu, L. Ji, H. Chao, Dalton Transactions, 45 (2016) 10546-10555.

[19] H. Deng, J. Cai, H. Xu, H. Zhang, L.-N. Ji, Dalton Transactions, (2003) 325-330.

[20] F. Gao, H. Chao, F. Zhou, Y.-X. Yuan, B. Peng, L.-N. Ji, Journal of inorganic biochemistry, 100 (2006) 1487-1494.

[21] C. Tan, S. Lai, S. Wu, S. Hu, L. Zhou, Y. Chen, M. Wang, Y. Zhu, W. Lian, W. Peng, L. Ji, A. Xu, Journal of Medicinal Chemistry, 53 (2010) 7613-7624.

[22] Y. Xiong, X.-F. He, X.-H. Zou, J.-Z. Wu, X.-M. Chen, L.-N. Ji, R.-H. Li, J.-Y. Zhou, K.-B. Yu, Journal of the Chemical Society, Dalton Transactions, (1999) 19-24.

[23] A.E. Friedman, J.C. Chambron, J.P. Sauvage, N.J. Turro, J.K. Barton, Journal of the American Chemical Society, 112 (1990) 4960-4962.

[24] S.S. Bhat, V.K. Revankar, A. Khan, R.J. Butcher, K. Thatipamula, New Journal of Chemistry, 39 (2015) 3646-3657.

[25] R.B.P. Elmes, M. Erby, S.A. Bright, D.C. Williams, T. Gunnlaugsson, Chemical Communications, 48 (2012) 2588-2590.

[26] M.P. Coogan, V. Fernandez-Moreira, Chemical Communications, 50 (2014) 384-399.

[27] V. Fernandez-Moreira, F.L. Thorp-Greenwood, M.P. Coogan, Chemical Communications, 46 (2010) 186-202.

[28] N.A. O'Connor, N. Stevens, D. Samaroo, M.R. Solomon, A.A. Marti, J. Dyer, H. Vishwasrao, D.L. Akins, E.R. Kandel, N.J. Turro, Chemical Communications, (2009) 2640-2642.

[29] M. Matson, F.R. Svensson, B. Nordén, P. Lincoln, The Journal of Physical Chemistry B, 115 (2011) 1706-1711.

[30] H. Huang, P. Zhang, Y. Chen, K. Qiu, C. Jin, L. Ji, H. Chao, Dalton Transactions, 45 (2016) 13135-13145.

[31] S.S. Bhat, A.S. Kumbhar, A.A. Kumbhar, A. Khan, P. Lonnecke, E. Hey-Hawkins, Chem Commun (Camb), 47 (2011) 11068-11070.

[32] S.S. Bhat, A.S. Kumbhar, P. Lönnecke, E. Hey-Hawkins, Inorganic Chemistry, 49 (2010) 4843-4853.

[33] S.S. Bhat, V.K. Revankar, A. Khan, R.V. Pinjari, M. Necas, Chem Asian J, 12 (2017) 254-264.

[34] S.S. Bhat, V.K. Revankar, R.V. Pinjari, N. S, C. Bogar, K. Bhat, V.A. Kawade, New Journal of Chemistry, 41 (2017) 5513-5520.

[35] S.S. Bhat, A.S. Kumbhar, A.A. Kumbhar, A. Khan, Chemistry – A European Journal, 18 (2012) 16383-16392.

[36] M.S. Deshpande, A.A. Kumbhar, A.S. Kumbhar, M. Kumbhakar, H. Pal, U.B. Sonawane, R.R. Joshi, Bioconjugate Chemistry, 20 (2009) 447-459.

[37] N. Nickita, G. Gasser, P. Pearson, M.J. Belousoff, L.Y. Goh, A.M. Bond, G.B. Deacon, L. Spiccia, Inorganic Chemistry, 48 (2009) 68-81.

[38] P.A. Anderson, G.B. Deacon, K.H. Haarmann, F.R. Keene, T.J. Meyer, D.A. Reitsma, B.W. Skelton, G.F. Strouse, N.C. Thomas, Inorganic Chemistry, 34 (1995) 6145-6157.

[39] J.-Z. Wu, B.-H. Ye, L. Wang, L.-N. Ji, J.-Y. Zhou, R.-H. Li, Z.-Y. Zhou, Journal of the Chemical Society, Dalton Transactions, (1997) 1395-1402.

[40] D.P. Rillema, D.S. Jones, C. Woods, H.A. Levy, Inorganic Chemistry, 31 (1992) 2935-2938.

[41] D.A. Freedman, J.K. Evju, M.K. Pomije, K.R. Mann, Inorganic Chemistry, 40 (2001) 5711-5715.

[42] M. R. Waterland, K. C. Gordon, J. J. McGarvey, P. M. Jayaweera, Journal of the Chemical Society, Dalton Transactions, (1998) 609-616.

[43] Q.-X. Zhou, W.-H. Lei, J.-R. Chen, C. Li, Y.-J. Hou, X.-S. Wang, B.-W. Zhang, Chemistry – A European Journal, 16 (2010) 3157-3165.

[44] A. Juris, V. Balzani, F. Barigelletti, S. Campagna, P. Belser, A. von Zelewsky, Coordination Chemistry Reviews, 84 (1988) 85-277.

[45] C. Sentagne, J.-C. Chambron, J.-P. Sauvage, N. Paillous, Journal of Photochemistry and Photobiology B: Biology, 26 (1994) 165-174.

[46] J. Sherborne, S.M. Scott, K.C. Gordon, Inorganica Chimica Acta, 260 (1997) 199-205.

[47] G. Bryant, J. Fergusson, Australian Journal of Chemistry, 24 (1971) 275-286.

[48] M.K. Nazeeruddin, S.M. Zakeeruddin, K. Kalyanasundaram, The Journal of Physical Chemistry, 97 (1993) 9607-9612.

[49] P.P. Pellegrini, J.R. Aldrich-Wright, Dalton Transactions, (2003) 176-183.

[50] S.S. Bhat, N. Shivalingegowda, V.K. Revankar, N.K. Lokanath, M.S. Kugaji, V. Kumbar, K. Bhat, Journal of Inorganic Biochemistry, 177 (2017) 127-137.

[51] S.P. Foxon, C. Green, M.G. Walker, A. Wragg, H. Adams, J.A. Weinstein, S.C. Parker, A.J.H.M. Meijer, J.A. Thomas, Inorganic Chemistry, 51 (2012) 463-471.

[52] A.E. Friedman, C.V. Kumar, N.J. Turro, J.K. Barton, Nucleic Acids Research, 19 (1991) 2595-2602.

[53] A. Chouai, S.E. Wicke, C. Turro, J. Bacsa, K.R. Dunbar, D. Wang, R.P. Thummel, Inorganic Chemistry, 44 (2005) 5996-6003.

[54] R.B. Nair, E.S. Teng, S.L. Kirkland, C.J. Murphy, Inorganic Chemistry, 37 (1998) 139-141.

[55] X.W. Liu, J. Li, H. Deng, K.C. Zheng, Z.W. Mao, L.N. Ji, Inorganica Chimica Acta, 358 (2005) 3311-3319.

[56] M.-J. Han, L.-H. Gao, K.-Z. Wang, New Journal of Chemistry, 30 (2006) 208-214.

[57] Y. Jenkins, A.E. Friedman, N.J. Turro, J.K. Barton, Biochemistry, 31 (1992) 10809-10816.

[58] R.B.P. Elmes, J.A. Kitchen, D.C. Williams, T. Gunnlaugsson, Dalton Transactions, 41 (2012) 6607-6610.

[59] M.J. Waring, Journal of Molecular Biology, 13 (1965) 269-282.

[60] J.M. Kelly, A.B. Tossi, D.J. McConnell, C. OhUigin, Nucleic Acids Research, 13 (1985) 6017-6034.

[61] G.A. Neyhart, N. Grover, S.R. Smith, W.A. Kalsbeck, T.A. Fairley, M. Cory, H.H. Thorp, Journal of the American Chemical Society, 115 (1993) 4423-4428.

[62] E.C. Long, J.K. Barton, Accounts of Chemical Research, 23 (1990) 271-273.

[63] S. Satyanarayana, J.C. Dabrowiak, J.B. Chaires, Biochemistry, 31 (1992) 9319-9324.

[64] H. Ahmad, D. Ghosh, J.A. Thomas, Chemical Communications, 50 (2014) 3859-3861.

[65] S. Mahadevan, M. Palaniandavar, Inorganic Chemistry, 37 (1998) 693-700.

[66] V. Rajendiran, M. Murali, E. Suresh, M. Palaniandavar, V.S. Periasamy, M.A. Akbarsha, Dalton Transactions, (2008) 2157-2170.

[67] N.B. Koji Nakanishi, Robert W. Woody, Circular Dichroism: Principles and Applications, VCH, New York, 1994.

[68] Y. Masaki, T. Yoshihito, Y. Yasuyuki, K. Shigeyasu, S. Ichiro, Bulletin of the Chemical Society of Japan, 65 (1992) 1006-1011.

[69] J.G. Collins, A.D. Sleeman, J.R. Aldrich-Wright, I. Greguric, T.W. Hambley, Inorganic Chemistry, 37 (1998) 3133-3141.

[70] J. Dickeson, L. Summers, Australian Journal of Chemistry, 23 (1970) 1023-1027.

[71] Dirk G. Kurth, Katharina M. Fromm, J.-M. Lehn, European Journal of Inorganic Chemistry, 2001 (2001) 1523-1526.

[72] D.P. Rillema, R.A. Kirgan, C. Moore, S. Koshy, Acta Crystallographica Section E, 63 (2007) o3526.

[73] I.P. Evans, A. Spencer, G. Wilkinson, Journal of the Chemical Society, Dalton Transactions, (1973) 204-209.

[74] S.M. Zakeeruddin, M.K. Nazeeruddin, R. Humphry-Baker, M. Grätzel, V. Shklover, Inorganic Chemistry, 37 (1998) 5251-5259.

[75] J.V. Caspar, T.J. Meyer, Journal of the American Chemical Society, 105 (1983) 5583-5590.

Scheme/Figure, Tables Captions

Scheme 1. Synthetic route for complexes **1–3**.

Figure 1. ORTEP diagram of the cations of complexes (a) **1** and (b) **3;** anions and solvent molecules are omitted for clarity. All ellipsoids are drawn at 50% probability level.

Figure 2. Cyclic voltammograms obtained at platinum working electrode for oxidation of complex **1** (1 mM) oxidation (top) and reduction (bottom) in acetonitrile (0.1 M tetrabutylammonium hexafluorophosphate (TBA)PF_6) for different scan rates.

Figure 3. UV-Visible spectroelectrochemical responses of complex **1** (30 µM) in acetonitrile (0.1 M tetrabutylammonium hexafluorophosphate (TBA)PF_6), during oxidation.

Figure 4. HOMO-LUMO energy level diagram for $[Ru(bpy)_3]^{2+}$, $[Ru(bpy)_2(dppz)]^{2+}$ and complexes **1-3**.

Figure 5. Emission spectra of complexes (a) **1**, (b) **2**, (c) **3**, 20 µM in phosphate buffer, pH 7.2, at 298 K with increasing [CT-DNA]/[Ru] ratio 0-30, (d) plot of relative integrated emission intensity versus [CT-DNA]/[Ru] for the complexes (□) **1**, (□) **2**, (□) **3**.

Figure 6. Effect of increasing amounts of complexes **1-3** and ethidium bromide (EtBr) on the relative viscosity of calf-thymus DNA at 28.0 °C, [DNA] = 300 µM.

Figure 7. CD spectra of CT-DNA in the presence and absence of complexes **1-3** in phosphate buffer (pH 7.2) [DNA]/[Complex] = 4, [DNA] = 200µM.

Figure 8. Cytotoxicity of complexes **1-3** against HL-60 cell line evaluated by MTT assay. (a) Time-dependent, [complex] =5µM (b) Concentration-dependent, [complex] =2-10µM. Results are mean values of three identical experiments.

Figure 9. Cytotoxicity of complexes **1-3** against HeLa cell line evaluated by MTT assay, (a) time-dependent, [complex] =5µM (b) concentration dependent, [complex] =2-10µM. Results are mean values of three identical experiments.

Figure 10. Fluorescence microscopy images of HL-60 (10^3) cells incubated (24 h) with 5 µM of complexes **2**, **3** and DNA-specific stain DAPI, (**a**) with complex **2** (left), DAPI (centre), overlay image (right); (**b**) with complex **3** (left), DAPI (centre), overlay image (right).

Figure 11. Fluorescence microscopy images of HeLa cells incubated (24 h) with 5 µM of complexes **2** or **3** and DNA-specific stain DAPI; (a) cells incubated with complex **2** (left),

DAPI (centre), overlay image (right); (b) cells incubated with complex **3** (left), DAPI (centre), overlay image (right). Images were taken after 24 h of incubation.

Table 1 Selected bond lengths [Å] and angles [°] for complex **1**

Table 2 Selected bond lengths [Å] and angles [°] for complex **3**

Table 3 UV/Vis and emission data for complexes **1**–**3**

Table 4 Electrochemical data for complexes in Acetonitrile

Table 5 Electronic absorption data of complexes **2** and **3** upon addition of CT-DNA

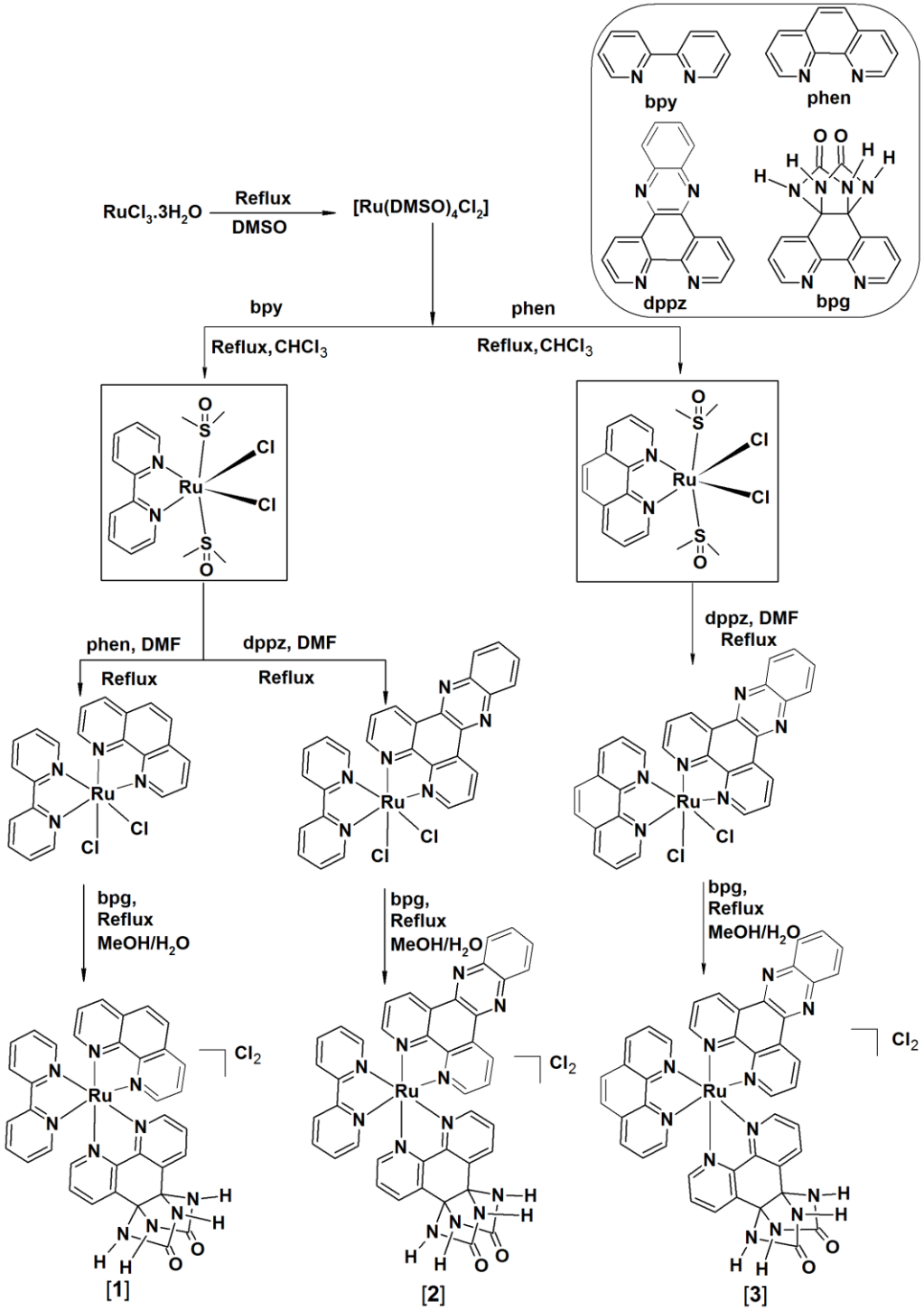
RuCl3.3H2O
Reflux
DMSO
[Ru(DMSO)4Cl2]
bpy
phen
dppz
bpg
bpy
phen
Reflux, CHCl3
Reflux, CHCl3
phen, DMF
Reflux
dppz, DMF
Reflux
dppz, DMF
Reflux
bpg,
Reflux
MeOH/H2O
bpg,
Reflux
MeOH/H2O
bpg,
Reflux
MeOH/H2O
Cl2
Cl2
Cl2
[1]
[2]
[3]

Scheme 1.

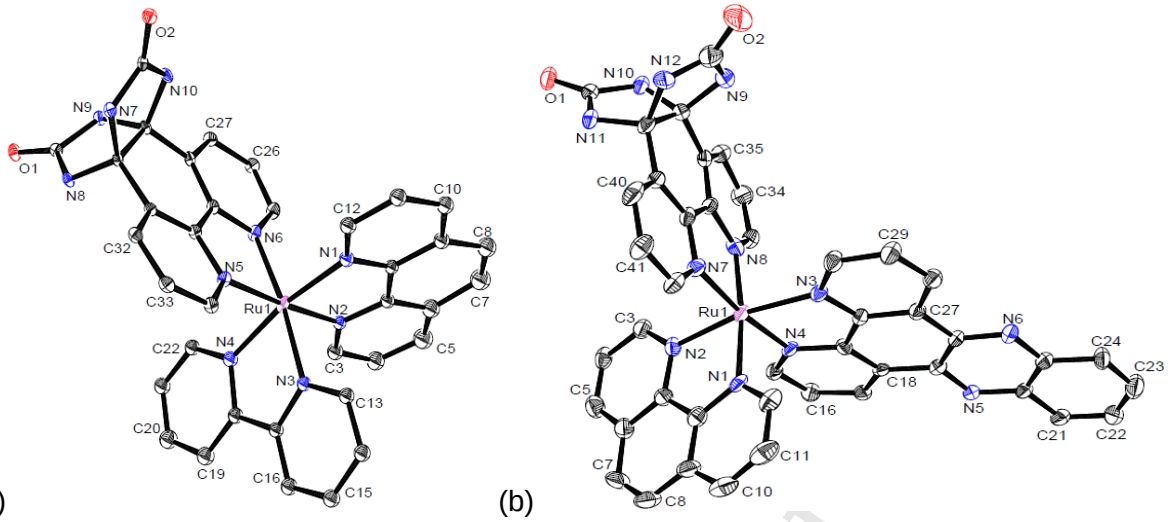

(a) (b)

Figure 1.

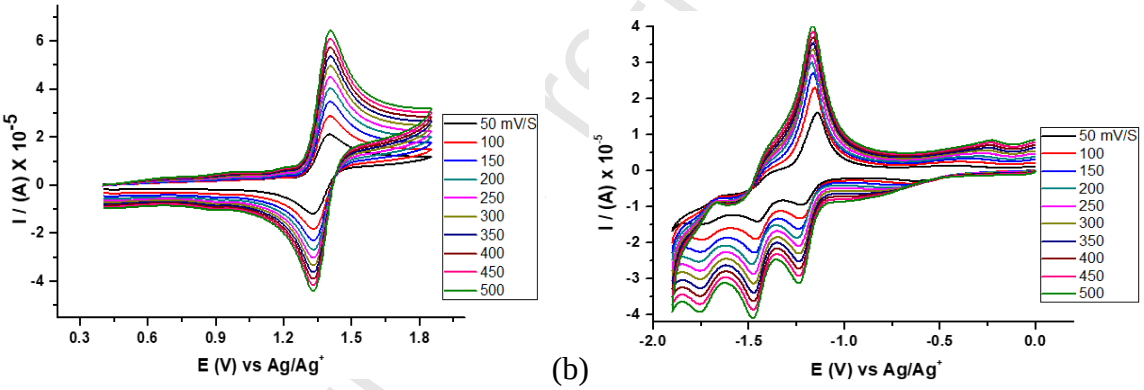

(a) (b)

Figure 2.

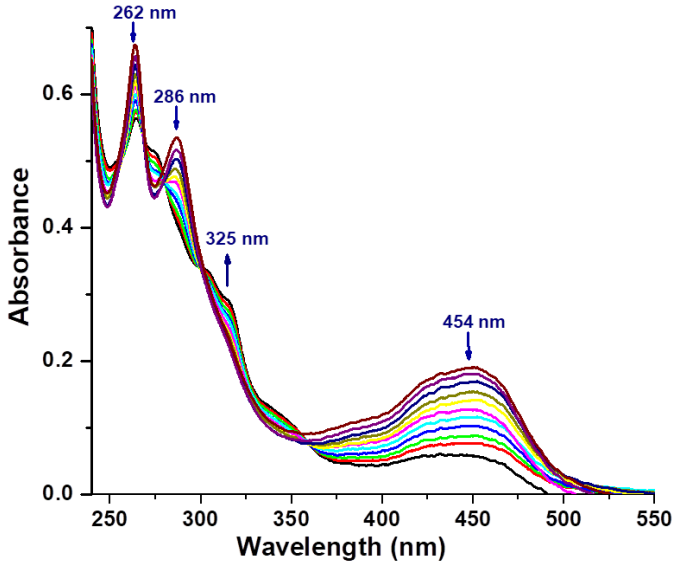

Figure 3.

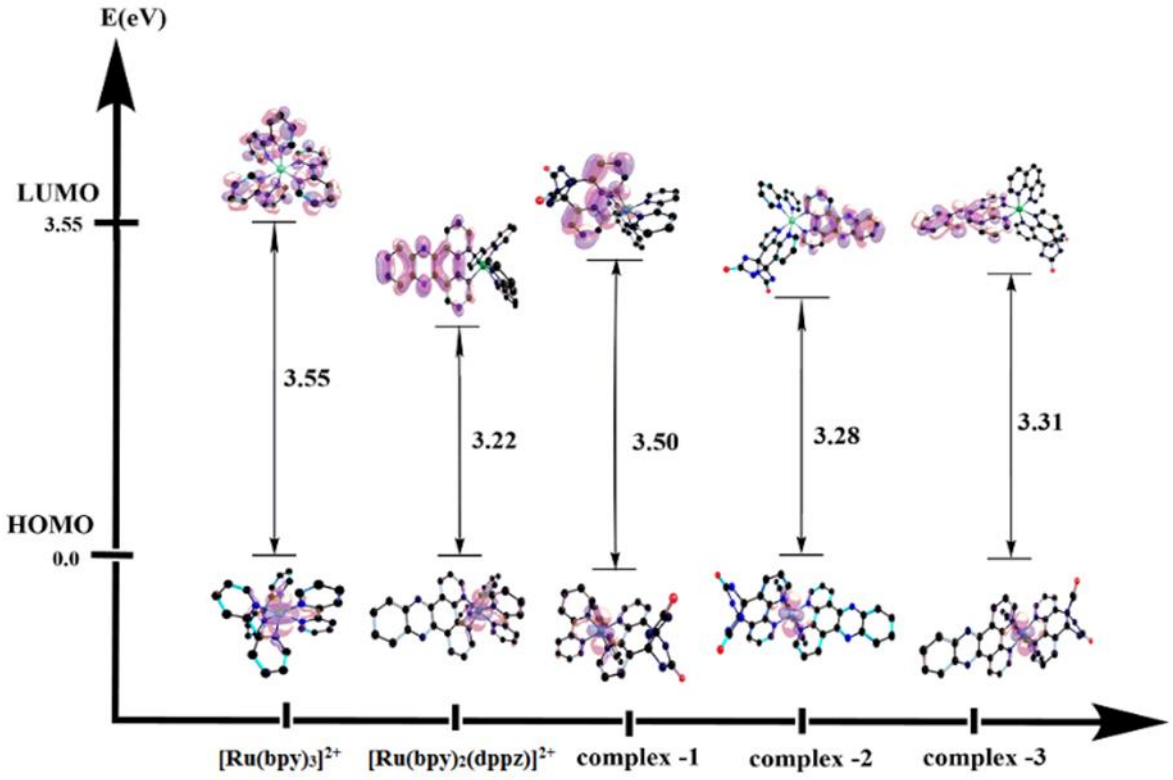

Figure 4.

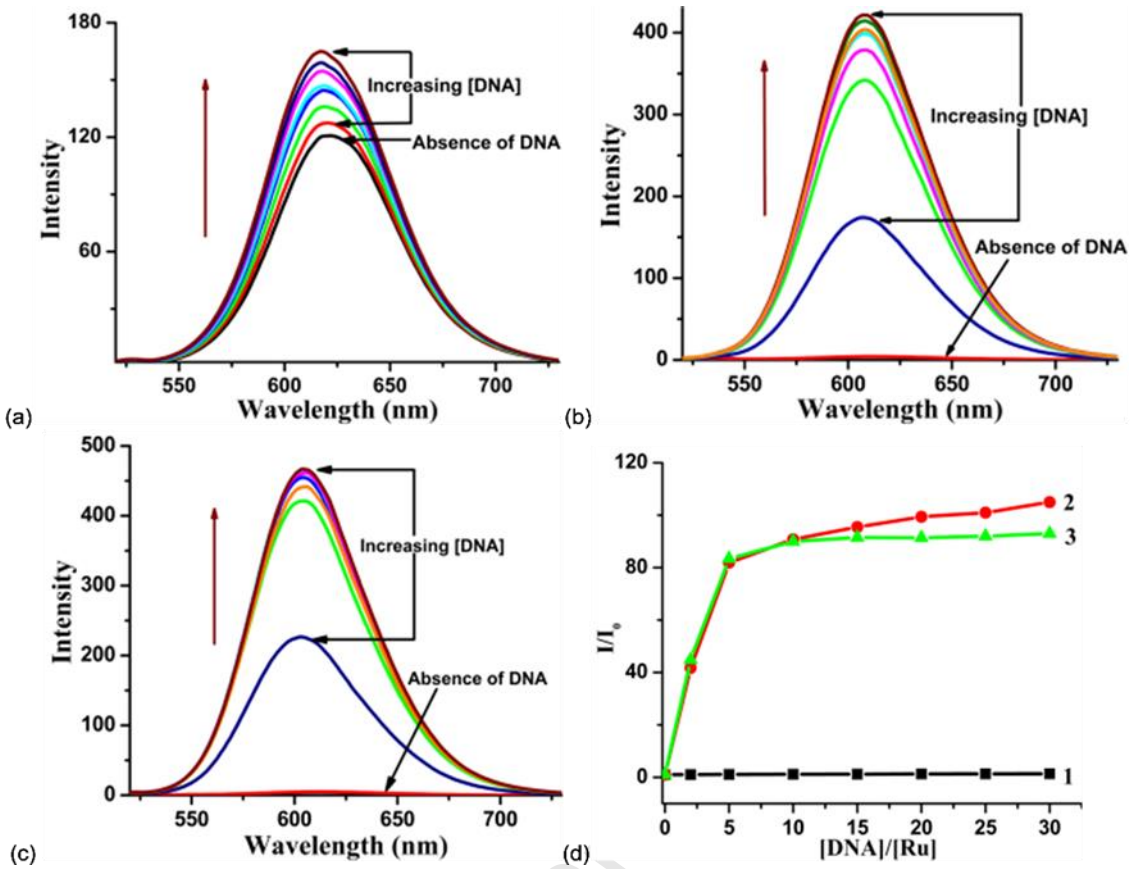

Figure 5.

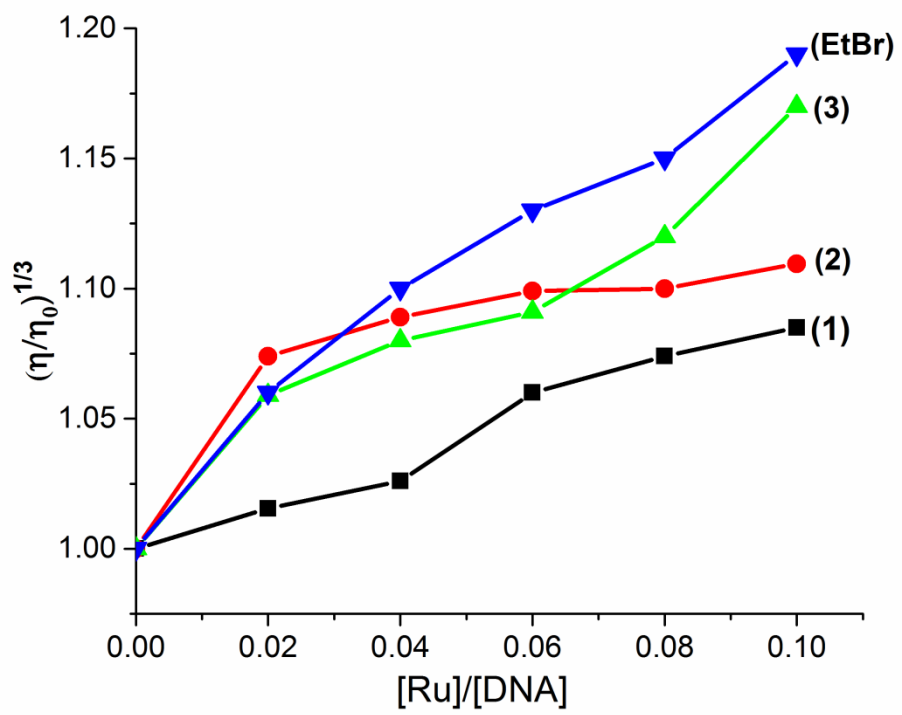

Figure 6.

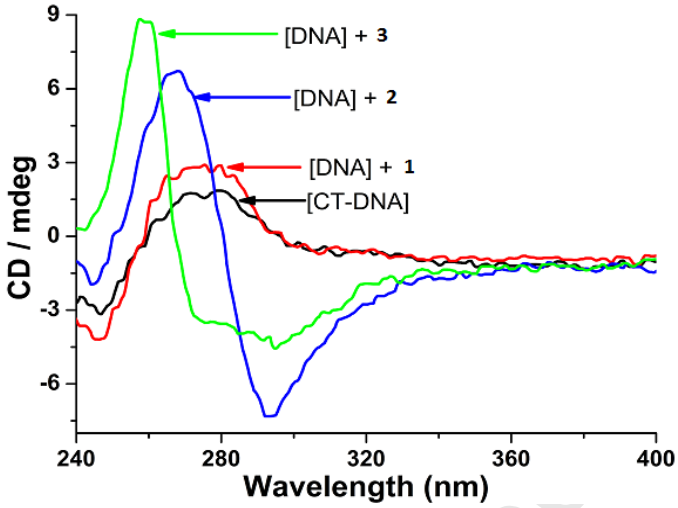

Figure 7.

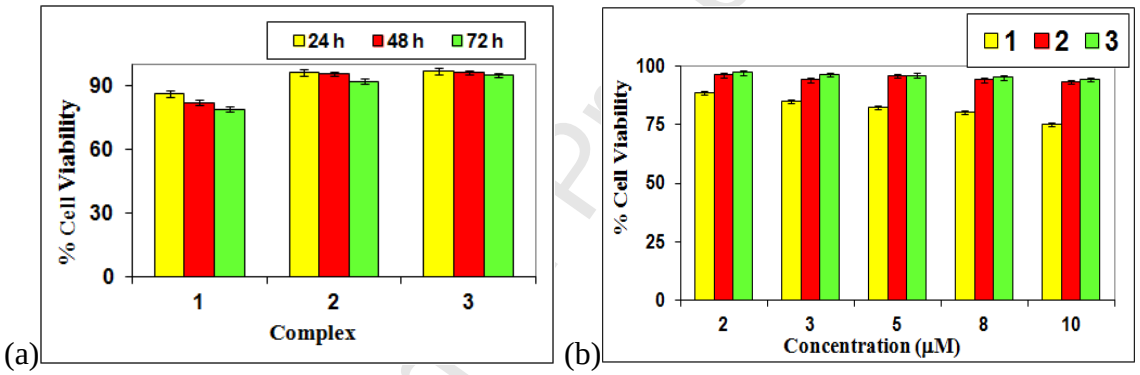

Figure 8.

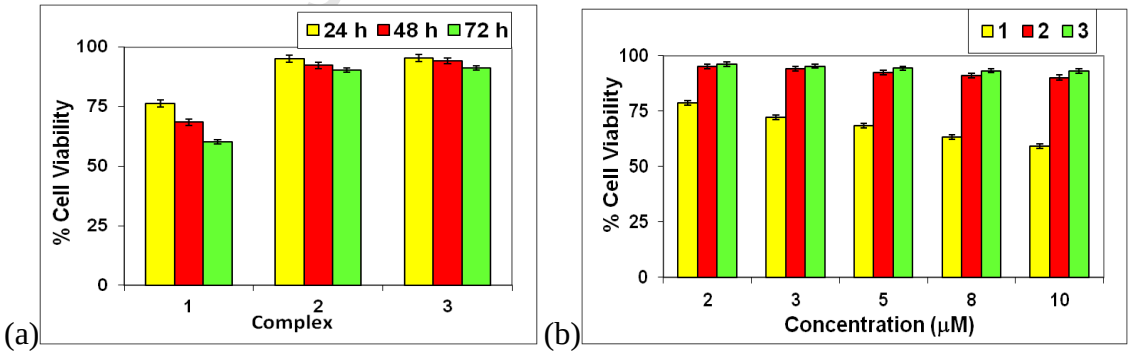

Figure 9.

(a)

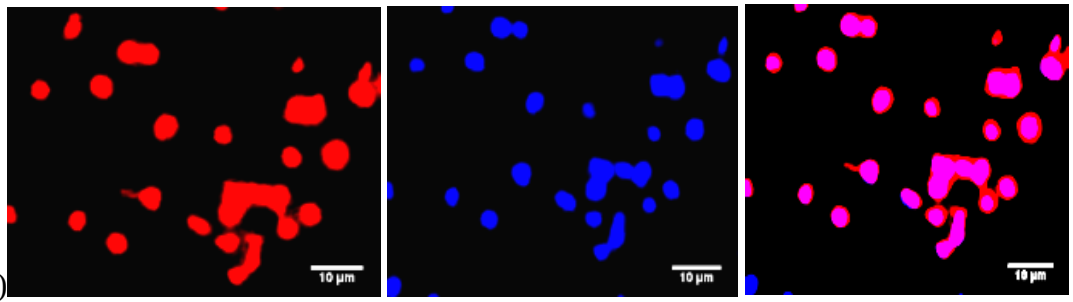

(b)

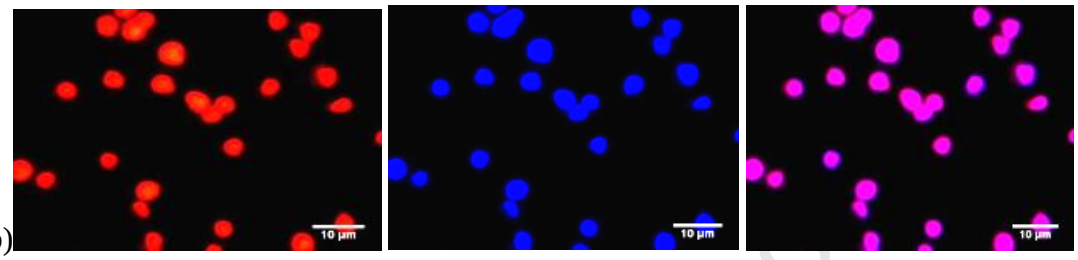

Figure 10.

(a)

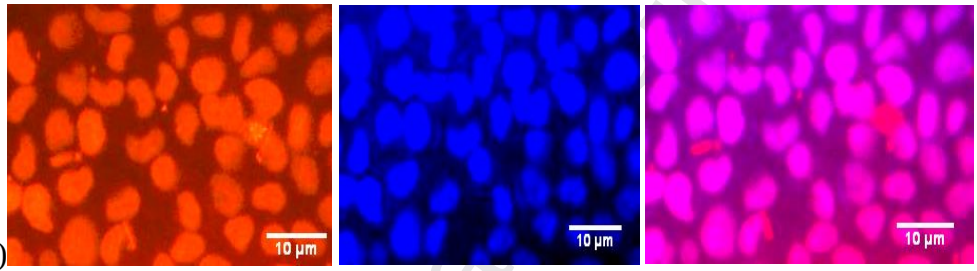

(b)

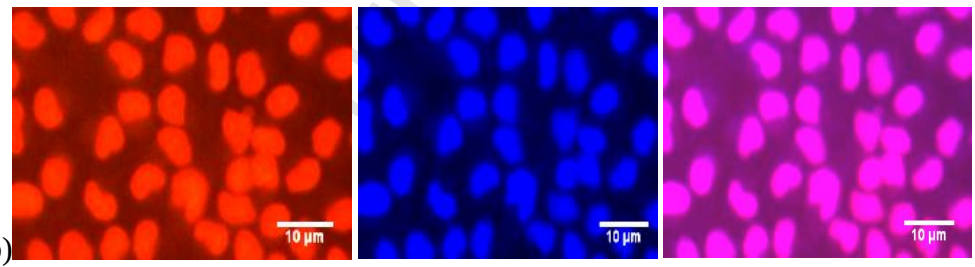

Figure 11.

Table 1 Selected bond lengths [Å] and angles [°] for complex **1.**

Bond lengths			
Ru(1)-N(1)	2.060(3)	Ru(1)-N(4)	2.070(3)
Ru(1)-N(2)	2.066(3)	Ru(1)-N(5)	2.055(3)
Ru(1)-N(3)	2.077(3)	Ru(1)-N(6)	2.060(3)
Bond angles			
N(2)-Ru(1)-N(1)	83.00(3)	N(2)-Ru(1)-N(3)	84.4(2)
N(3)-Ru(1)-N(1)	96.50(2)	N(4)-Ru(1)-N(3)	75.80(3)
N(4)-Ru(1)-N(1)	170.70(3)	N(5)-Ru(1)-N(3)	99.2(1)
N(5)-Ru(1)-N(1)	95.20(3)	N(6)-Ru(1)-N(3)	172.8(2)
N(6)-Ru(1)-N(1)	90.7(1)	N(5)-Ru(1)-N(4)	91.1(2)
N(4)-Ru(1)-N(2)	91.0(2)	N(6)-Ru(1)-N(4)	97.10(2)
N(5)-Ru(1)-N(2)	176.2(1)	N(5)-Ru(1)-N(6)	79.1(1)
N(6)-Ru(1)-N(2)	97.5(1)		

Table 2 Selected bond lengths [Å] and angles [°] for complex **3.**

Bond Lengths			
Ru(1)-N(1)	2.067(4)	Ru(1)-N(4)	2.071(4)
Ru(1)-N(2)	2.068(4)	Ru(1)-N(7)	2.069(4)
Ru(1)-N(3)	2.059(4)	Ru(1)-N(8)	2.025(5)
Ru(2)-N(13)	2.094(9)	Ru(2)-N(16)	2.077(4)
Ru(2)-N(14)	2.069(8)	Ru(2)-N(19)	2.047(5)
Ru(2)-N(15)	2.066(4)	Ru(2)-N(20)	2.053(4)
Bond Angles			
N(2)-Ru(1)-N(1)	79.95(2)	N(8)-Ru(1)-N(3)	91.65(2)
N(3)-Ru(1)-N(1)	93.38(2)	N(8)-Ru(1)-N(7)	79.18(2)
N(4)-Ru(1)-N(1)	89.52(2)	N(3)-Ru(1)-N(7)	95.90(2)
N(7)-Ru(1)-N(1)	96.02(2)	N(2)-Ru(1)-N(7)	93.88(2)
N(8)-Ru(1)-N(1)	173.39(2)	N(8)-Ru(1)-N(4)	95.63(2)
N(3)-Ru(1)-N(2)	160.70(2)	N(3)-Ru(1)-N(4)	79.45(2)
N(4)-Ru(1)-N(2)	91.30(2)	N(7)-Ru(1)-N(4)	172.99(2)
N(8)-Ru(1)-N(2)	95.75(2)		
N(16)-Ru(2)-N(13)	92.0(3)	N(20)-Ru(2)-N(16)	174.62(2)

N(14)-Ru(2)-N(13)	77.8(4)	N(19)-Ru(2)-N(16)	95.79(2)
N(15)-Ru(2)-N(13)	87.4(3)	N(15)-Ru(2)-N(14)	163.5(3)
N(20)-Ru(2)-N(13)	92.7(3)	N(20)-Ru(2)-N(14)	90.4(3)
N(19)-Ru(2)-N(13)	172.1(3)	N(19)-Ru(2)-N(14)	100.2(3)
N(14)-Ru(2)-N(16)	93.2(3)	N(20)-Ru(2)-N(15)	97.67(2)
N(15)-Ru(2)-N(16)	79.93(2)	N(19)-Ru(2)-N(15)	95.42(2)
N(19)-Ru(2)-N(20)	79.58(2)		

Table 3 UV/Vis and emission data for complexes **1**–**3.**

Complex[a]	Absorbance $\lambda_{max}/\varepsilon$ ($M^{-1}cm^{-1}$) (Acetonitrile) Ligand MLCT transitions	Emission					
		λ_{em}[c]	ϕ_{em}[d]	λ_{em}[c]	ϕ_{em}[d]	λ_{em}[c]	[d]ϕ_{em}
		Acetonitrile		DMF		Water	
1	264/49945 286/35840 449/14015	616	0.075	619	0.065	635	0.022
2	278/76095 351/17690 454/16360	611	0.081	614	0.051	--	--
3	265/85370 366/17565 438/1607	610	0.095	616	0.047	--	--
[b][$Ru(bpy)_3$]$^{2+}$	--	606	0.063	601	0.062	603	0.042

[a] [Ru] = 10 (±0.2) μM, [b] data taken from ref.[75], error limit: λ_{max} = ± 2 nm, ε = ±2%, [c] emission maxima, [d] ϕ = emission quantum yield excited at 450 nm.

Table 4 Electrochemical data for complexes in Acetonitrile.

[a]Complex	Metal-based E^0_f in V	Ligand-based (V)		
$[Ru(bpy)_3]^{2+}$	0.88	-0.92	-1.12	-1.36
1	0.96	-0.79	-1.03	-1.30
2	0.99	-0.53	-1.07	-1.43
3	0.99	-0.48	-0.96	-1.18

[a] Data reported for 1 mM solutions in CH_3CN with $(TBA)PF_6$ as the supporting electrolyte. Scan rate was 100 mV/s, vs Fc/Fc^+, error limit: E^0_f = ± 0.01 V.

Table 5 Electronic absorption data of complexes **2** and **3** upon addition of CT-DNA.

Complex[a]	$\Delta\lambda_{max}$ (MLCT)	Hypochromism H (%) [b]			K_b (M^{-1})
2	10	14.9 (450)	18.2 (364)	24.0 (280)	2.3×10^4
3	4	16.1 (438)	32.0 (372)	16.0 (264)	6.8×10^4
[c]$[Ru(bpy)_2(dppz)]^{2+}$	-	14.5 (444)	40.1 (372)	-	5.0×10^6
[d]$[Ru(phen)_2(dppz)]^{2+}$	-	-	35 (370)	-	5.1×10^6
[e]$[Ru(NH_3)_4(dppz)]^{2+}$	-	13.6 (544)	-	-	1.2×10^5

[a] [DNA]: [Ru] = 7:1; [b] H % = $100(A_{free}-A_{bound})/A_{free}$ in phosphate buffer (pH = 7.2), where A = Absorbance; Error limit: λ_{max} = ± 2 nm, H (%) = ± 5%; K_b (M^{-1}) = ± 5%.[c] Data taken from ref.[13] . [d] Data taken from ref.[56]. [e] Data taken from ref.[56].

Graphical Abstract

Tris-Heteroleptic Ruthenium(II) Polypyridyl Complexes: Synthesis, Structural Characterization, Photophysics, Electrochemistry and Biological Properties

Novel non-toxic water soluble tris-heteroleptic ruthenium(II) complexes with cellular imaging properties have been described. The complexes show extensive "molecular light switch effect" for DNA.

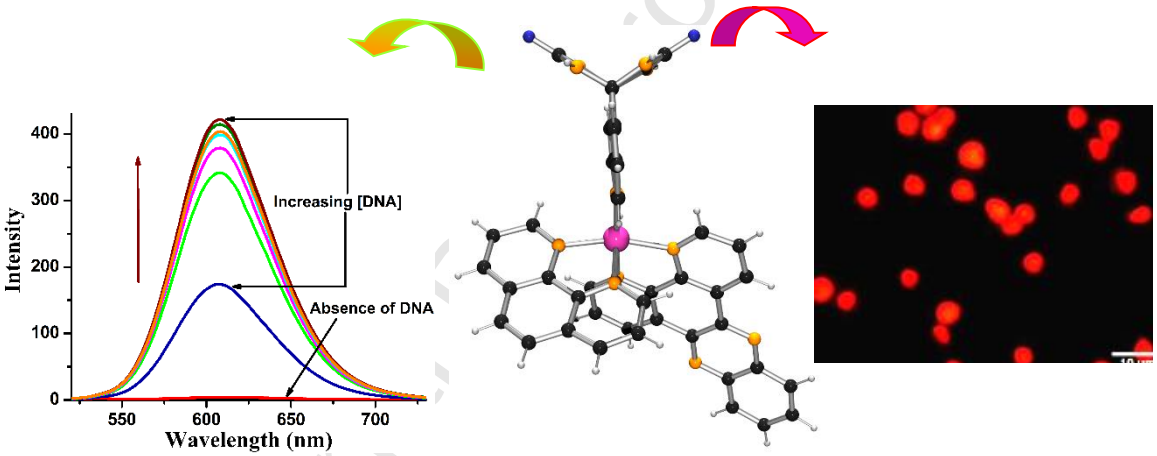

Highlights:

- Tris-heteroleptic Ru(II) polypyridyl complexes were synthesised and characterized.
- Complexes are water soluble and have good affinity for DNA.
- Complexes have solvent dependent photo-physical properties.
- The complexes show extensive "molecular light switch" effect for DNA
- These complexes are non-toxic and stain the nucleus of the cells.